Proc. Natl. Acad. Sci. USA
Vol. 95, pp. 7909–7914, July 1998
Biochemistry

Solution structure of the cytohesin-1 (B2–1) Sec7 domain and its interaction with the GTPase ADP ribosylation factor 1

STEPHEN F. BETZ*, ARNDT SCHNUCHEL*, HONG WANG*, EDWARD T. OLEJNICZAK*, ROBERT P. MEADOWS*, BRIAN P. LIPSKY†, EDITH A. S. HARRIS†, DONALD E. STAUNTON†, AND STEPHEN W. FESIK*‡

*Pharmaceutical Discovery Division, Abbott Laboratories, Abbott Park, IL 60064; and †ICOS Corporation, 22021 20th Avenue SE, Bothell, WA 98021

Edited by Kurt Wüthrich, Swiss Federal Institute of Technology, Zurich, Switzerland, and approved May 8, 1998 (received for review March 31, 1998)

ABSTRACT **Cytohesin-1 (B2–1) is a guanine nucleotide exchange factor for human ADP ribosylation factor (Arf) GTPases, which are important for vesicular protein trafficking and coatamer assembly in the cell. Cytohesin-1 also has been reported to promote cellular adhesion via binding to the β2 integrin cytoplasmic domain. The solution structure of the Sec7 domain of cytohesin-1, which is responsible for both the protein's guanine nucleotide exchange factor function and β2 integrin binding, was determined by NMR spectroscopy. The structure consists of 10 α-helices that form a unique tertiary fold. The binding between the Sec7 domain and a soluble, truncated version of human Arf-1 was investigated by examining ^{1}H-^{15}N and ^{1}H-^{13}C chemical shift changes between the native protein and the Sec7/Arf-1 complex. We show that the binding to Arf-1 occurs through a large surface on the C-terminal subdomain that is composed of both hydrophobic and polar residues. Structure-based mutational analysis of the cytohesin-1 Sec7 domain has been used to identify residues important for binding to Arf and for mediating nucleotide exchange. Investigations into the interaction between the Sec7 domain and the β2 integrin cytoplasmic domain suggest that the two proteins do not interact in the solution phase.**

G proteins are critical to several functions within the cell, including growth, proliferation, signal transduction, membrane trafficking, and cytoskeletal interactions (1). A common characteristic of G proteins is that they cycle between an active GTP-bound form and an inactive GDP-bound form. Cellular regulation of G proteins and GTPase activity occurs at both stages of this cycle. Proteins that accelerate GTP hydrolysis are termed GAPs (GTPase-activating proteins), and those that activate GTPases by promoting the substitution of GDP with GTP are termed GEFs (guanine nucleotide exchange factors).

The GEFs for two *Saccharomyces cerevisae* ADP ribosylation factors (Arfs) (2) and for human Arf-1 (3) recently were discovered. Arf proteins are a family of GTPases belonging to the Ras superfamily (4) and are critical to vesicular traffic through the Golgi (5), coatamer assembly (6), and phospholipase D activation (7, 8). Each of the Arf GEF proteins contain a homologous ≈200-residue region, the Sec7 domain, that alone has been shown to support guanine nucleotide exchange. This domain is named after the *S. cerevisae SEC7* gene product, which is required for proper protein transport through the Golgi (9, 10). Several Sec7 domain-containing proteins have since been identified (2, 11–14), including two homologs in humans (3, 15). The fungal and plant proteins are very large (>1,400 residues) and likely contain several protein modules. However, the human proteins are smaller and have three domains: a ≈55-residue coiled coil-containing domain, the Sec7 domain, and a ≈110-residue pleckstrin homology (PH) domain (Fig. 1). Although the Sec7 domain itself is sufficient to catalyze nucleotide exchange, the PH domain is thought to localize the protein to the membrane surface by binding phosphoinositides (13, 16–18). It is at the membrane surface that Sec7 catalyzes GDP → GTP exchange on Arf proteins *in vivo*. A similar process exists for the GTPase exchange factors in the Sos/Ras and Dbl/Rho families. Both of these GEFs (Sos and Dbl) contain PH domains that target the proteins to the membrane surface where they activate their respective substrates (19, 20).

Recently, the three-dimensional structures of a GEF bound to its G protein have been determined for Ef-Tu/EF-Ts from *Escherichia coli* (21) and *Thermus thermophilus* (22). Based on this structural information, a mechanism has been proposed in which EF-Ts (the GEF) binds to EF-Tu and disrupts the nucleotide binding site, prompting release of GDP. In the *E. coli* structure, the Mg^{2+} cofactor binding is disturbed, whereas in the *T. thermophilus* structure, EF-Ts binding results in a reorganization of the hydrogen bonding network of the phosphates, prompting release of the nucleotide. The structure of another exchange factor (GrpE) complexed to its target (ATPase domain of DnaK) also has been reported (23). This GEF acts by causing a conformational shift in DnaK, destabilizing the purine and ribose binding pockets. Thus, although they have evolved to perform the same function, GEFs have developed several mechanisms to accelerate nucleotide exchange.

Here, we report on the solution structure of the Sec7 domain from cytohesin-1. Cytohesin-1 is a human Sec7 domain-containing protein found primarily in immune system cells (13), which has been shown to be a GEF for both Arf-1 and Arf-3 (3, 24) and to interact with the β2 integrin cytoplasmic domain (CD18) (25). Based on the NMR-derived structure of the Sec7 domain and the chemical shift changes observed on binding to Arf-1, site-directed mutants of Sec7 were prepared and tested for their ability to bind Arf-1 and catalyze GDP → GTP exchange. We also have investigated the binding of CD18 to the cytohesin-1 Sec7 domain.

MATERIALS AND METHODS

Cloning, Mutagenesis, and Expression. The cytohesin-1 (B2–1) cDNA was isolated by PCR amplification from a human spleen cell cDNA library (26) using primers based on the B2–1 gene sequence (15). The gene was cloned into the

The publication costs of this article were defrayed in part by page charge payment. This article must therefore be hereby marked "*advertisement*" in accordance with 18 U.S.C. §1734 solely to indicate this fact.

This paper was submitted directly (Track II) to the *Proceedings* office.
Abbreviations: Arf, ADP ribosylation factor; HSQC, heteronuclear single-quantum coherence; GEF, guanine nucleotide exchange factor; NOE, nuclear Overhauser effect.
Data deposition: The structure reported in this paper has been deposited in the Protein Data Bank, Biology Department, Brookhaven National Laboratory, Upton, NY 11973 (PDB ID code 1bc9).
‡To whom reprint requests should be addressed. e-mail: fesiks@pprd.abbott.com.

FIG. 1. Domain composition of cytohesin-1 and other human homologs. Numbering refers to the primary sequence of cytohesin-1. CC, coiled coil-containing domain; Sec7, Sec7 domain; PH, pleckstrin homology domain.

*Nde*I–*Xho*I restriction sites of the expression vector pET-15b (Novagen). Residues 58–248 (the Sec7 domain) were subcloned into the *Nde*I–*Xho*I restriction sites of the expression vector pET-30b (Novagen). Site-directed mutagenesis was performed by using the Quickchange Mutagenesis Kit (Stratagene).

The Arf-1 cDNA was isolated by PCR amplification from a human spleen cell cDNA library (26) by using primers based on the Arf-1 sequence (27). The gene was cloned into the *Nde*I–*Xho*I restriction sites of the expression vector pET-15b (Novagen). Residues 18–181 (Δ17Arf-1) were subcloned into the *Nde*I–*Xho*I restriction sites of pET-20b. (Novagen). All vector sequences were confirmed by dye-terminator DNA sequencing by using an Applied Biosystems Prism 300 Genetic Analyzer (Perkin–Elmer).

Proteins were expressed in *E. coli* BL21(DE3) or BL21(DE3)pLysS (Novagen). Uniformly labeled ^{15}N or ^{15}N,^{13}C-labeled protein samples were prepared by growing transformed *E. coli* in minimal media containing $^{15}NH_4Cl$, with or without [U-^{13}C]-glucose (Cambridge Isotope Laboratories, Cambridge, MA). Uniformly ^{15}N,^{13}C-labeled, fractionally deuterated proteins were prepared in a similar fashion by using 75% ^2H_2O. Additionally, ^{15}N-perdeuterated and 15% ^{13}C-labeled proteins were prepared. The proteins containing polyhistidine tails were purified by affinity chromatography using ProBond metal binding resin (Invitrogen). Chemically synthesized cytoplasmic β2 integrin domain (see ref. 25 for sequence) was purchased through a commercial supplier (PeptidoGenic, Livermore, CA).

NMR Spectroscopy. NMR sample buffer conditions were 25 mM NaP_i, 150 mM $(NH_4)_2SO_4$, 3 mM DTT, pH 6.8, and protein concentrations were 700 μM 1 mM. NMR spectra were acquired at 305 K on Bruker DRX500, DRX600, AMX750, or DRX800 NMR spectrometers. Deuterium-decoupled backbone ^1H-^{15}N-^{13}C triple-resonance spectra [HNCA, HN(CO)CA, HN(CA)CB, HN(COCA)CB, HNCO, HN(CA)CO] of cytohesin-1 Sec7 domain were obtained with a ^{15}N,^{13}C-labeled sample that was 75% deuterated (28). HCCH total correlation spectroscopy experiments were recorded by using a ^{15}N,^{13}C-labeled sample in ^2H_2O buffer (29). Distance restraints were obtained from ^{15}N- or ^{13}C-resolved nuclear Overhauser effect (NOE) spectra (30, 31), and ϕ dihedral angle restraints were measured from $^3J_{HNH\alpha}$ coupling constants (32). Hydrogen-deuterium exchange experiments were performed by diluting a concentrated sample of the cytohesin-1 Sec7 domain with NMR buffer containing ^2H_2O. This sample was concentrated to 800 μM, and ^1H-^{15}N-heteronuclear single-quantum coherence (HSQC) spectra were recorded as a function of time.

To examine protein–protein binding, mixtures with equimolar amounts (≈750 μM) of ^{15}N,^{13}C-labeled cytohesin-1 Sec7 domain and unlabeled Δ17Arf-1 were prepared. The samples were dialyzed versus the cytohesin-1 NMR buffer overnight at 4°C. Two-dimensional ^1H-^{15}N- and ^1H-^{13}C-HSQC spectra of the mixtures were acquired and compared with those of native cytohesin-1 Sec7 domain.

To investigate CD18/Sec7 domain binding, the peptide corresponding to the β2 integrin cytoplasmic domain was dissolved in 25 mM NaP_i (pH 6.8), dispensed into 1-, 2-, or 5-mg aliquots, and lyophilized. These lyophilates were titrated directly into NMR samples of the cytohesin-1 Sec7 domain. Two-dimensional ^1H-^{15}N- and ^1H-^{13}C-HSQC spectra of the mixtures were acquired and compared with those of native cytohesin-1 Sec7 domain.

Structure Calculations. Solution structures were calculated by using a distance geometry/simulated annealing protocol (33) with the program X-PLOR 3.1 (34). A square-well potential (F_{NOE} = 50 kcal mol^{-1}) was used to restrain NOE-derived distances. NOE restraints were categorized into four groups (1.8–3.0 Å, 1.8–4.0 Å, 1.8–5.0 Å, or 1.8–5.5 Å) based on NOE crosspeak intensity. Crosspeaks that were not resolved clearly were assigned to the 1.8–5.5 Å category. Torsional restraints were applied to ϕ angles of -120 ± 30 degrees for $^3J_{HNH\alpha}$ coupling constants ≥8.5 Hz and -60 ± 30 degrees for coupling constants ≤5.5 Hz. Torsional restraints for the latter were applied only in α-helical regions. A force constant of 200 kcal mol^{-1}·rad^{-2} were applied to all torsional restraints. Hydrogen bonds were included only in α-helices, and only if the H^N was slowly exchanging in the hydrogen-deuterium exchange experiment and the residue possessed appropriate short-range NOE restraints. Each hydrogen bond was defined by two distance restraints: 1.8–2.3 Å for O-H and 2.8–3.3 Å for O-N. The quality of the geometry of the structures was evaluated by using the program PROCHECK-NMR (35).

Nucleotide Exchange Assay. Nucleotide exchange was monitored by using a modified version of the protocol of Paris *et al.* (36). The cytohesin-1 Sec7 domain (or variant) was mixed with a 100-fold excess of Δ17Arf-1 at 37°C in a 200-μl reaction in 50 mM Hepes (pH 7.5), 1 mM DTT, 1 mM $MgCl_2$, 100 mM KCl, and 10 μM (^{35}S)GTPγS (3–6 × 10^6 cpm/reaction). At minute intervals, samples were removed and quenched by dilution into 2 ml of ice-cold 20 mM Hepes (pH 7.5), 100 mM NaCl, and 10 mM $MgCl_2$. Diluted samples were filtered by using 25-mm, 0.45-μm BA nitrocellulose filters (Schliecher & Schull). The filters were washed twice with ice-cold quench buffer, dried, and counted. First-order reaction rate constants (k) were determined by fitting the amount of GTPγS bound (A) as a function of time (t) using the equation $A = A_f(1 - e^{-kt})$, where A_f is the amount of GTPγS bound at infinite time.

RESULTS AND DISCUSSION

Structure Determination. The ^1H, ^{15}N, and ^{13}C backbone resonances of the cytohesin-1 Sec7 domain were assigned by correlating ^1H-^{15}N pairs from each *i* residue with the $^{13}C^\alpha$, $^{13}C^\beta$, and $^{13}C'$ resonances of the *i* and *i-1* residues using a set of three-dimensional triple-resonance experiments (28). HCCH total correlation spectroscopy experiments were used to assign the side chain ^1H and ^{13}C resonances (29). The prochiral methyl groups of Val and Leu were stereospecifically assigned by using a 15% ^{13}C-labeled sample as described by Neri *et al.* (37).

A total of 2,135 NOE-derived distance restraints, 56 explicit hydrogen bonds (112 restraints), and 44 ϕ dihedral angle restraints were used to determine the protein's structure. Fifty-two of 278 (19%) XPLOR-calculated structures exhibited a total energy ≤200 kcal mol^{-1}. The 20 structures with the lowest energies were included in the ensemble (Fig. 2*a*). The rms deviation of the ensemble is 1.0 Å for backbone atoms and 1.5 Å for all heavy atoms. The structural statistics for the ensemble and energy-minimized average structure are presented in Table 1. The structures are energetically stable and have no distance violation greater than 0.4 Å. Fig. 2 *b* and *c* represents alignments of the N-terminal (residues 60–135) and C-terminal (residues 136–245) subdomains, respectively. Each domain is well defined individually (see Table 1) compared with the entire protein because of variations in the orientation between the two subdomains caused by the paucity of inter-subdomain NOEs.

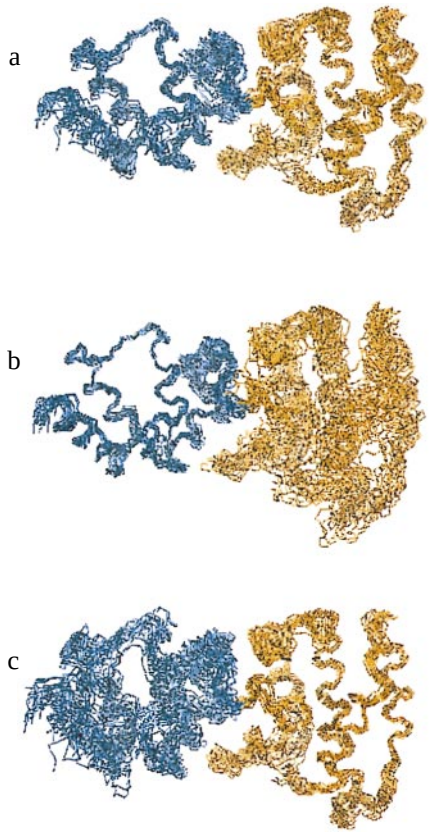

FIG. 2. Backbone atom superposition of 20 cytohesin-1 Sec7 domain structures. The N-terminal subdomain (residues 58–135) is shown in blue. The C-terminal subdomain (residues 136–248) is shown in gold. (*a*) Superposition over the whole protein (residues 60–245). (*b*) Superposition of the N-terminal subdomain. (*c*) Superposition of the C-terminal subdomain. The unstructured polyhistidine tag at the very C terminus is not pictured for clarity.

A Ramachandran plot of the backbone angles for the averaged minimized structure shows that most (91.1%) of the backbone geometries lie within energetically favorable regions (Fig. 3). For the ensemble, 93.5% of the 3,600 nonglycyl, nonprolyl backbone angles fall within allowed regions. The residues that have backbone dihedral angles consistently in disallowed regions (R153, Q181, D226, L227, and F244) are in poorly defined loops.

The Cytohesin-1 Sec7 Domain Structure. The primary sequence, secondary structure, and local distance restraints for cytohesin-1 are presented in Fig. 4. The protein is composed of two five α-helix subdomains and forms an extended (rather than globular) shape (Fig. 5). The N-terminal subdomain begins with α1 (residues 61–75). This is followed by a short Asp-Pro loop that connects this helix with α2 (residues 78–86) to form an antiparallel helix pair. Residues 87–93 form an extended loop that terminates in α3 (residues 94–102). Two short loops connect α3 to α4 (residues 109–115) and α4 to α5 (residues 121–129). Overall, the helices in these first $\approx$75 residues form a compact, right-turning superhelical bundle.

The C-terminal subdomain begins with α6 (residues 141–146), a six-residue helix. This short helix is connected to α7 (residues 160–172) via a long loop that is highly conserved throughout Sec7 domain sequences. A short, overhand loop leads to α8 (residues 184–200), the longest α-helix in the protein ($\approx$25 Å). A 10-residue loop terminates at α9 (residues 211–221), which forms an antiparallel pair with α8. The last α-helix, α10 (residues 229–241), crosses over the α8-α9 helix pair at a $\approx$60° angle. Finally, the C terminus of the Sec7 domain (residues 242–248) exits the protein after making contact with the loop between α6 and α7. The two subdomains are connected sequentially by the loop between α5 and α6. NOE distance restraints between α4 and the long loop preceding α7 and contacts between α5 and α7 comprise the few intersubdomain interactions.

Table 1. Structural statistics for cytohesin-1 Sec7 domain

	⟨SA⟩	⟨SA⟩$_r$
rmsd (Å) from experimental distance restraints		
Interresidue long (581)	0.012 ± 0.002	0.013
Interresidue short (422)	0.016 ± 0.001	0.014
Interresidue sequential (576)	0.012 ± 0.003	0.011
Intraresidue (556)	0.008 ± 0.002	0.005
Hydrogen bonds (112)	0.019 ± 0.002	0.018
XPLOR energies (kcal mol^{-1})*		
E_{total}	162.1 ± 4.3	150.3
E_{bonds}	7.1 ± 0.4	6.5
E_{angles}	98.5 ± 2.2	91.5
E_{vdw}	28.7 ± 2.1	30.1
E_{impr}	8.2 ± 0.7	7.0
E_{NOE}	19.4 ± 2.7	15.2
E_{cdih}	0.08 ± 0.06	0.01
$E_{L\text{-}J}$	−1,062 ± 19	−979
Cartesian coordinate rmsd (Å)†	Backbone	All heavy
Protein (residues 60–245)	1.0 ± 0.3	1.5 ± 0.3
N-terminal domain (residues 60–135)	0.7 ± 0.2	1.3 ± 0.2
C-terminal domain (residues 136–245)	0.8 ± 0.2	1.3 ± 0.2

⟨SA⟩ is the ensemble of 20 structures, ⟨SA⟩$_r$ is the energy-minimized mean atomic structure. rmsd, rms deviation.

*Energies were calculated by using XPLOR as described in *Materials and Methods*. $E_{L\text{-}J}$ was not used during refinement, but is included here as an independent assessment of nonbonded geometry.

†Atomic rmsd between the 20 NMR ensemble structures and the mean atomic structure coordinates after superposition of backbone heavy atoms (N, C$^{\alpha}$, C′) or all nonhydrogen atoms.

Fig. 6 depicts the solvent-accessible surface of the cytohesin-1 Sec7 domain. The yellow patch at the top of the molecule presented in Fig. 6*a* represents the largest hydrophobic surface on the protein. It is composed of residues from α8 and α9 and

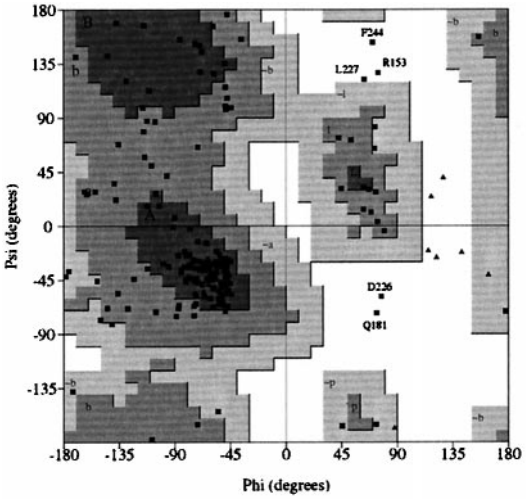

FIG. 3. PROCHECK-NMR-generated (35) Ramachandran plot for the energy minimized, average structure of the cytohesin-1 Sec7 domain. Residues with geometries outside of acceptable regions are indicated. Shaded areas marked by uppercase, lowercase, and lowercase residues with a "~" prefix refer to most favored, favored, and allowed backbone geometries, respectively.

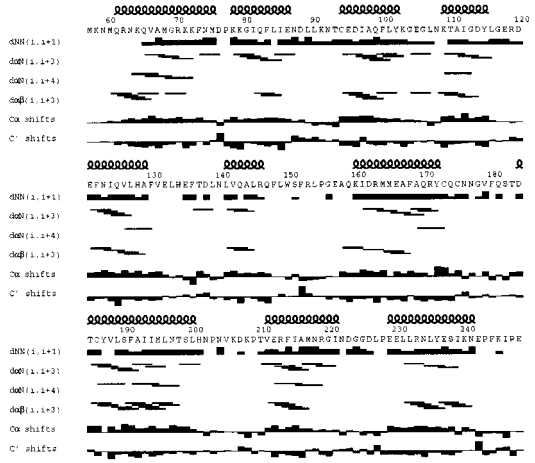

FIG. 4. Primary sequence and secondary structure of the cytohesin-1 Sec7 domain. Local ^{1}H homonuclear NOE restraints [$d_{NN}(i, i+1)$, $d_{\alpha N}(i, i+3)$, $d_{\alpha N}(i, i+4)$, $d_{\alpha\beta}(i, i+3)$] and deviations from random coil chemical shifts for $^{13}C^{\alpha}$ and $^{13}C'$ that define the secondary structure are indicated (38).

is surrounded by several charged residues. On the opposite face of the protein (Fig. 6*b*), the yellow patch near the top left shows a smaller hydrophobic surface that consists of residues in the loop between α7 and α8.

***β*2 Integrin Cytoplasmic Domain Binding.** Kolanus *et al.* (25) have reported that cytohesin-1 binds to the cytoplasmic domain of β2 integrin and that its Sec7 domain is responsible for this interaction. *In vivo*, overexpression of cytohesin-1, or its Sec7 domain alone, promotes adhesion of Jurkat cells to intracellular adhesion molecule (ICAM)-1-coated dishes presumably through $\alpha_L\beta_2$ integrin activation. To gain structural insight into this interaction, we compared the NMR spectra of the cytohesin-1 Sec7 domain in the presence and absence of CD18. A peptide corresponding to the β2 cytoplasmic domain sequence described by Kolanus *et al.* (25) was synthesized and titrated into a sample of ^{15}N,^{13}C-labeled cytohesin-1 Sec7 domain. After each addition of CD18, ^{1}H-^{15}N- and ^{1}H-^{13}C-HSQC spectra were acquired. No changes in the Sec7 domain spectra occurred even at 5:1 peptide/protein mixtures ([cytohesin-1] = 500 μM), indicating that no binding occurred (K_d > 1 mM). Fluorescence-monitored binding experiments conducted under several experimental conditions (data not shown) were consistent with the NMR studies and showed that no binding between the peptide and the protein was occurring. These results apparently contradict those of Kolanus *et al.* (25) in which the cytohesin-1 Sec7 domain was shown to bind to

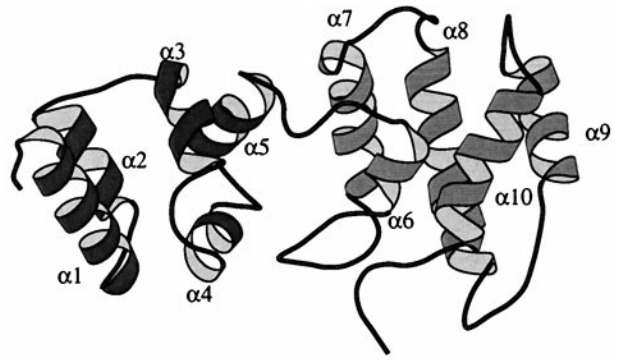

FIG. 5. MOLSCRIPT (39) diagram of the structure of the cytohesin-1 Sec7 domain. The N-terminal subdomain (residues 58–135) is shaded in dark gray, and the C-terminal subdomain (residues 136–248) is shown in light gray. The unstructured polyhistidine tag at the C terminus has been excluded for clarity.

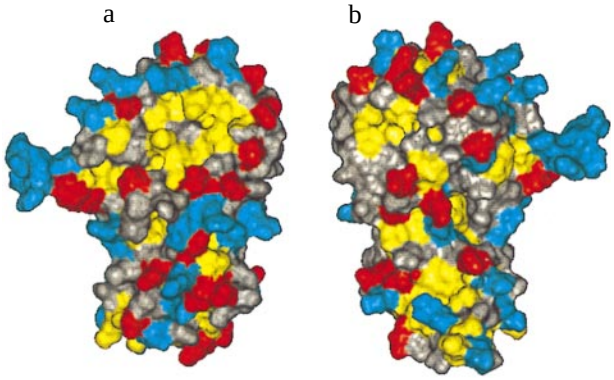

FIG. 6. Solvent-accessible surface area of the cytohesin-1 Sec7 domain. (*a*) Surface colored by residue characteristics: yellow is hydrophobic (Leu, Ile, Val, Met, Phe), red is acidic (Asp, Glu), and blue is basic (Lys, Arg, His). All other residue types are colored gray. (*b*) 180° rotated view showing the opposite face of the protein.

CD18-derivatized Sepharose with a K_d = 2.5 μM. It may be possible that this discrepancy is caused by differences in the way that the binding experiments were conducted, one in the solid phase and the other in solution.

Δ17Arf-1 Binding. Sec7 domains have been reported to be exchange factors for Arf GTPase proteins (2, 3, 18, 24). To model the interactions between Sec7 domains and Arf proteins, we probed the binding of the cytohesin-1 Sec7 domain to Δ17Arf-1 (36). This water-soluble Arf variant lacks the membrane-interacting myristoyl group and N-terminal α-helix. Δ17Arf-1 no longer requires phospholipid vesicles for Sec7 proteins to accelerate the exchange of GDP → GTP (36). ^{15}N,^{13}C-labeled cytohesin-1 Sec7 domain and unlabeled Δ17Arf-1 were mixed in a 1:1 complex, and ^{1}H-^{15}N- and ^{1}H-^{13}C-HSQC spectra were acquired and compared with those of the native Sec7 domain.

Fig. 7 illustrates the residues in the cytohesin-1 Sec7 domain that display ^{1}H-^{13}C and ^{1}H-^{15}N chemical shift changes on the binding of Δ17Arf-1. The data indicate that Δ17Arf-1 is interacting with the C-terminal subdomain of Sec7. This binding face is composed mainly of residues from α6 and the loop that follows as well as α8 and α9. Inspection of Sec7 domain primary sequences (2, 3, 11–15) indicates that α8 and the loop after α6 are the most conserved regions within the Sec7 domain. The opposite side of the protein (Fig. 7*b*) contains fewer residues that display ^{1}H-^{13}C chemical shift changes. The changes that occur on this face of the molecule

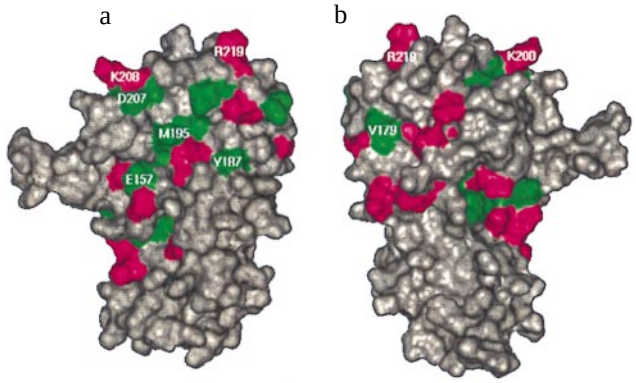

FIG. 7. Surface of the cytohesin-1 Sec7 domain colored by chemical shift changes on binding to Δ17Arf-1: green indicates residues that have chemical shift changes >0.05 ppm in ^{1}H and/or >0.25 ppm in ^{13}C, magenta indicates residues that have chemical shift changes >0.05 ppm in ^{1}H and/or >0.25 ppm in ^{15}N. The orientations are identical to those in Fig. 6. The sites of mutations are annotated.

are localized mostly to a small, hydrophobic pocket (Fig. 6*b*) and the loop following α6.

Mutagenesis. Based on the Sec7 domain structure, the observed chemical shift changes, and the primary sequence homology of Sec7 domains, several surface mutants of the Sec7 domain were designed to examine Arf binding and nucleotide exchange. The residues that were mutated are indicated on the surface of the cytohesin-1 Sec7 domain in Fig. 7. E157 was selected for mutation because of the large chemical shift changes observed for this residue and results from previous studies in which a Glu → Lys mutant at the homologous position of *Arabidopsis thaliana* EMB30 Sec7 domain causes defects in cell division, elongation, and adhesion (12). To investigate the importance of a negative charge at this position, E157 was mutated to a Ala (neutral) and a Lys (positive charge). Y187 and M195 were selected for mutation because they are part of the hydrophobic patch central to the Δ17Arf-1 binding surface (Figs. 6*a* and 7*a*). The charged residues D207, K208, and R219 that surround the hydrophobic patch were chosen for mutation to test the necessity of polar interactions, and V179 was chosen to test whether the smaller hydrophobic surface on the opposite protein face (Figs. 6*b* and 7*b*) is critical for Δ17Arf-1 binding.

For each of the mutants, ^{15}N-labeled NMR samples were prepared and their ^{1}H-^{15}N-HSQC spectra were compared with that of the native cytohesin-1 Sec7 domain. For all of the mutant proteins, chemical shift differences were restricted to a few residues near the mutations, demonstrating that the mutant proteins are folded correctly and do not exhibit any mutant-induced conformational changes.

Fig. 8 depicts the nucleotide exchange activity of the mutant proteins. The efficiency of GDP → GTP exchange on Δ17Arf-1 decreased for all of the mutant proteins and decreased by ≈90% or more for four mutant proteins. The mutants that have catalytic efficiencies <10% that of the wild-type are E157A, E157K, Y187A, and M195A. NMR binding experiments were conducted to examine whether the greatly decreased activity of these mutants was accompanied by a concomitant decrease in binding affinity for Δ17Arf-1. Three of the variants (E157K, Y187A, and M195A) do not bind appreciably to Δ17Arf-1 as indicated by the lack of any chemical shift changes on the addition of Δ17Arf-1. Surprisingly however, the same chemical shift changes observed for the wild-type protein also were observed for the E157A mutant, indicating that this nonfunctional mutant binds to Δ17Arf-1 in a manner similar to the native protein. These results suggest that E157 may not only be important for binding to Arf proteins, but that this residue is also critical for the catalytic function of the Sec7 domain.

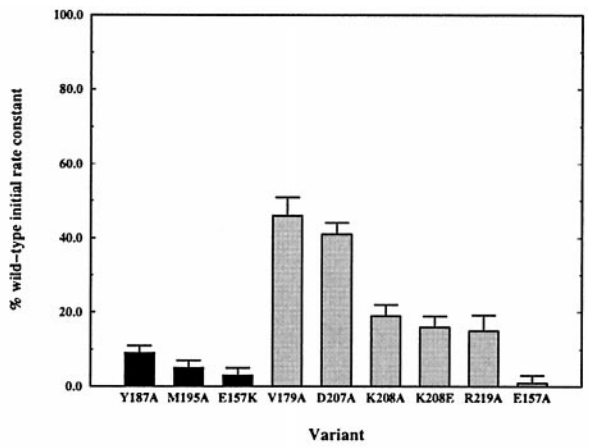

FIG. 8. The percentage of wild-type initial nucleotide exchange rate of cytohesin-1 Sec7 domain variants. The black columns represent proteins that do not bind to Δ17Arf-1 in an NMR binding assay. The gray columns represent proteins that bind to Δ17Arf-1.

Other mutant proteins were made to probe the importance of regions peripheral to the major hydrophobic surface. The D207A, K208A/E, and R219A variants decrease exchange activity from 50–80%, suggesting that the Δ17Arf-1 binding face is composed of both hydrophobic and polar/electrostatic components. Interestingly, the V179A mutation, designed to test the importance of the small hydrophobic surface (Fig. 6*b*), causes a ≈50% decrease in the initial rate of exchange activity. Although this decrease is less than the effects observed for other more critical hydrophobic residues (M195A and Y187A), it suggests that this hydrophobic surface also could be involved in nucleotide exchange.

Comparison with Other Proteins. Sec7 domains bear no significant sequence homology to other protein sequences, including other exchange factors. In addition, the three-dimensional structure of the cytohesin-1 Sec7 domain reported here does not resemble any known structure when compared with the Protein Data Bank by using the program DEJAVU (40). Thus, the Sec7 domain fold represents a unique tertiary structure. Interestingly, the C-terminal subdomain (residues 136–250) of Sec7 bears a topological and functional similarity to the catalytic domain of RasGAP-334 (41) in that both are elongated α-helical structures that affect the bound nucleotide of a GTPase.

During the preparation of this paper, two crystal structures of the Sec7 domain of a homologous protein, ARNO, were published (42, 43). The two proteins possess a high degree of sequence homology (83% identical) and the structures of the Sec7 domains of cytohesin-1 in solution and ARNO in the crystalline form are similar. Each has 10 α-helices organized in a similar overall topology. However, there are differences in the lengths of some of the helices. For example, α3, α5, and α6 in ARNO are 2–4 residues longer than in the NMR structure of cytohesin-1 (there is also disagreement about the length of α6 between the two crystal structures). Moreover, α7 is more than a full helical turn longer in ARNO than in cytohesin-1. The largest structural difference between the two proteins is at the C terminus of α9. In cytohesin-1, this α-helix is extended by five residues when compared with ARNO, which results in a difference in the loop structure between α9 and α10.

CONCLUSIONS

We have determined the solution structure of the Sec7 domain of cytohesin-1. The protein consists of 10 α-helices that form an extended structure composed of two subdomains. We examined the binding between the Sec7 domain and human Arf-1 by observing ^{1}H-^{15}N and ^{1}H-^{13}C chemical shift changes of the native protein on the addition of a water-soluble Arf-1 variant (Δ17Arf-1). We show that the binding to Arf-1 occurs exclusively through the C-terminal subdomain and that the binding surface is composed of both hydrophobic and polar residues. Using site-directed mutagenesis, we identified residues that are important for nucleotide exchange and Arf binding, which indicate the most important regions are the loop between α6 and α7 and a large area composed of residues from α8 and α9. We also have identified a mutant protein (E157A) that binds to Δ17Arf-1, but is unable to catalyze nucleotide exchange, suggesting that E157 may be involved in the catalytic mechanism of this enzyme.

Some of the NMR studies described in this paper were carried out at the National Magnetic Resonance Facility at Madison (operation subsidized by the National Institutes of Health (NIH) Biomedical Research Technology Program under Grant RR02301; equipment funded by the University of Wisconsin, National Science Foundation (NSF) Academic Infrastructure Program under Grant BIR-9214394, the NIH Shared Instrumentation Program under Grants RR02781 and

RR08438, the NIH Biomedical Research Technology Program under NIH Grant RR02301, the NSF Biological Instrumentation Program under Grant DMB-8415048, and the U.S. Department of Agriculture).

1. Bourne, H. R., Sanders, D. A. & McCormick, F. (1991) *Nature (London)* **349,** 117–127.
2. Peyroche, A., Paris, S. & Jackson, C. L. (1996) *Nature (London)* **384,** 479–481.
3. Chardin, P., Paris, S., Antonny, B., Robineau, S., Béraud-Dufour, S., Jackson, C. L. & Chabre, M. (1996) *Nature (London)* **384,** 481–484.
4. Boman, A. L. & Kahn, R. A. (1995) *Trends Biochem. Sci.* **20,** 147–150.
5. Rothman, J. E. & Ocri, L. (1992) *Nature (London)* **355,** 409–415.
6. Salama, N. R. & Scheckman, R. W. (1995) *Curr. Opin. Cell Biol.* **7,** 536–543.
7. Brown, H. A., Gutowski, S., Moomaw, C. R., Slaughter, C. & Sternweis, P. C. (1993) *Cell* **75,** 1137–1144.
8. Cockcroft, S., Thomas, G. M. H., Fensome, A., Geny, B., Cunningham, E., Gout, I., Hiles, I., Totty, N. F., Truong, O. & Hsuan, J. J. (1994) *Science* **263,** 523–526.
9. Novick, P., Ferro, S. & Scheckman, R. (1981) *Cell* **25,** 461–469.
10. Achstetter, T., Franzusoff, A., Field, C. & Scheckman, R. (1988) *J. Biol. Chem.* **263,** 11711–11717.
11. Wilson, R., Ainscough, R., Anderson, K., Baynes, C., Berks, M., Bonfield, J., Burton, J., Connell, M., Copsey, T., Cooper, J., *et al.* (1994) *Nature (London)* **368,** 32–38.
12. Shevell, D. E., Leu, W.-M., Gillmour, C. S., Xia, G., Feldmann, K. A. & Chua, N.-H. (1994) *Cell* **77,** 1051–1062.
13. Klarlund, J. K., Guilherme, A., Holik, J. J., Virbasius, J. V., Chawla, A. & Czech, M. P. (1997) *Science* **275,** 1927–1930.
14. Telemenakis, I., Benseler, F., Stenius, K., Südhof, T. C. & Brose, N. (1997) *Eur. J. Cell Biol.* **74,** 143–149.
15. Liu, L. & Pohajdak, B. (1992) *Biochem. Biophys. Acta* **1132,** 75–78.
16. Harlan, J. E., Yoon, H. S., Hajduk, P. J. & Fesik, S. W. (1995) *Biochemistry* **34,** 9859–9864.
17. Rameh, L. E., Arvidsson, A., Carraway III, K. L., Couvillon, A. D., Rathbun, G., Crompton, A., VanRenterghem, B., Czech, M. P., Ravichandran, K. S., Burakoff, S. J., *et al.* (1997) *J. Biol. Chem.* **272,** 22059–22066.
18. Klarlund, J. K., Rameh, L. E., Cantley, L. C., Buxton, J. M., Holik, J. J., Sakelis, C., Patki, V., Corvera, S. & Czech, M. P. (1997) *J. Biol. Chem.* **273,** 1859–1862.
19. Porifiri, E., Evans. T., Chardin, P. & Hancock, J. F. (1994) *J. Biol. Chem.* **269,** 22672–22677.
20. Cerione, R. A. & Zheng, Y. (1996) *Curr. Opin. Cell Biol.* **8,** 216–222.
21. Kawashima, T., Berthet-Colominas, C., Wulff, M., Cusack, S. & Leberman, R. (1996) *Nature (London)* **379,** 511–518.
22. Wang, Y., Jiang, Y., Meyering-Voss, M., Sprinzl, M. & Sigler, P. B. (1997) *Nat. Struct. Biol.* **4,** 650–656.
23. Harrison, C. J., Hayer-Hartl, M., Di Liberto, M., Hartl, F. U. & Kuriyan, J. (1997) *Science* **276,** 431–435.
24. Meacci, E., Tsai, S.-C., Adamik, R., Moss, J. & Vaughn, M. (1997) *Proc. Natl. Acad. Sci. USA* **94,** 1745–1748.
25. Kolanus, W., Nagel, W., Schiller, B., Zeitimann, L., Godar, S., Stockinger, H. & Seed, B. (1996) *Cell* **86,** 233–242.
26. Van der Vieren, M., Le Trong, H., Wood, C. L., Moore, P. F., St. John, T., Staunton, D. E. & Gallitin, W. M. (1995) *Immunity* **3,** 683–690.
27. Kahn, R. A., Kern, F. G., Clark, J., Gelmann, E. P. & Rulka, C. (1991) *J. Biol. Chem.* **266,** 2606–2614.
28. Yamazaki, T., Lee, W., Arrowsmith, C. H., Muhandiram, D. R. & Kay, L. E. (1994) *J. Am. Chem. Soc.* **116,** 11655–11666.
29. Clore, G. M. & Gronenborn, A., M. (1994) *Methods Enzymol.* **239,** 349–363.
30. Fesik, S. W. & Zuiderweg, E. R. P. (1988) *J. Magn. Reson.* **78,** 588–593.
31. Marion, D., Driscoll, P. C., Kay, L. E., Wingfield, P. T., Bax, A., Gronenborn, A. M. & Clore, G. M. (1989) *Biochemistry* **29,** 6150–6156.
32. Kuboniwa, H., Grzesiek, S., Delaglio, F. & Bax, A. (1994) *J. Biomol. NMR* **4,** 871–878.
33. Kuszewski, J., Nilges, M. & Brünger, A. T. (1992) *J. Biomol. NMR* **2,** 33–56.
34. Brünger, A. T. (1992) X-PLOR Version 3.1 Manual (Yale University, New Haven, CT).
35. Laskowski, R. A., MacArthur, M. W., Moss, D. S. & Thornton, J. M. (1993) *J. Appl. Cryst.* **26,** 283–291.
36. Paris, S., Béraud-Dufour, S., Robineau, S., Bigay, J., Antonny, B., Chabre, M. & Chardin, P. (1997) *J. Biol. Chem.* **272,** 22221–22226.
37. Neri, D., Szyperski, T., Otting, G., Senn, H. & Wüthrich, K. (1989) *Biochemistry* **28,** 7510–7516.
38. Spera, S. & Bax, A. (1991) *J. Am. Chem. Soc.* **113,** 5490–5492.
39. Kraulis, P. (1991) *J. Appl. Cryst.* **24,** 946–950.
40. Kleywegt, G. J. & Jones, T. A. (1995) *Structure* **3,** 535–540.
41. Scheffzek, K., Ahmadian, M. R., Kabsch, W., Wiesmüller, L., Lautwein, A., Schmitz, A. & Wittinghofer, A. (1997) *Science* **277,** 333–338.
42. Mossessova, E., Gulbis, J. M. & Goldberg, J. (1998) *Cell* **92,** 415–423.
43. Cherfils, J., Ménétrey, J., Mathieu, M., Le Bras, G., Robineau, S., Béraud-Dufour, S., Antonny, B. & Chardin, P. (1998) *Nature (London)* **392,** 101–105.